Experimental validation of exoplanet centring strategies for high dispersion coronagraphy

Mona El Morsy, Arthur Vigan, Maxime Lopez, Gilles Otten, Élodie Choquet, Fabrice Madec, Anne Costille, Jean-François Sauvage, Kjetil Dohlen, Eduard Muslimov, et al.

Experimental validation of exoplanet centring strategies for high dispersion coronagraphy

M. El Morsy[a], A. Vigan[a], M. Lopez[a], G. P. P. L. Otten[a,b], É. Choquet[a], F. Madec[a], A. Costille[a], J.-F. Sauvage[a,c], K. Dohlen[a], E. Muslimov[a,d,e], R. Pourcelot[a,f], J. Floriot[a], J.-A. Benedetti[a], P. Blanchard[a], P. Balard[a], and G. Murray[g]

[a]Aix Marseille Univ, CNRS, CNES, LAM, Marseille, France
[b]Academia Sinica, Institute of Astronomy and Astrophysics, 11F Astronomy-Mathematics Building, NTU/AS campus, No. 1, Section 4, Roosevelt Rd., Taipei 10617, Taiwan
[c]DOTA, ONERA, Université Paris Saclay (COmUE)
[d]NOVA Optical IR Instrumentation Group at ASTRON Oude Hoogeveensedijk 4, 7991 PD Dwingeloo, The Netherlands
[e]Kazan National Research Technical University named after A.N. Tupolev KAI, 10 K. Marx, Kazan, Russia, 420111
[f]Université Côte d'Azur, Observatoire de la Côte d'Azur, CNRS, Laboratoire Lagrange, Bd de l'Observatoire, CS 34229, 06304, Nice Cedex 4, France
[g]Center for Advanced Instrumentation, Durham University, Durham, DH1 3LE, United Kindgom

ABSTRACT

The combination on large ground-based telescopes of extreme adaptive optics (ExAO), coronagraphy and high-dispersion spectroscopy is starting to emerge as a powerful technique for the direct characterisation of giant exoplanets. High spectral resolution not only brings a major gain in terms of accessible spectral features, but it also enables to better disentangle between the stellar and planetary signals thanks to the much higher spectral content. On-going projects such as KPIC for Keck, REACH for Subaru and HiRISE for the VLT base their observing strategy on the use of a few science fibres, one of which is dedicated to sampling the PSF of the planet, while the others sample the stellar residuals in the speckle field. The main challenge in this approach is to blindly centre the science fibre on the planet's PSF, with typically a tolerance of less than one resolution element ($0.1\,\lambda/D$). Several possible centring strategies can be adopted, either based on calibration fibres retro-injecting signal to mark the position of the science fibres or based on the use of focal-plane features introduced by the ExAO system. In this proceeding, we describe different possible approaches and we compare their centring accuracy using the MITHiC high-contrast imaging testbed. For this work, MITHiC has been upgraded to reproduce a setup close to the one that will be adopted in HiRISE, the coupling system that will soon be implemented between VLT/SPHERE and VLT/CRIRES+. Our results demonstrate that reaching a specification accuracy of $0.1\,\lambda/D$ is extremely challenging regardless of the chosen centring strategy. It requires a high level of accuracy at every step of the centring procedure, which can be reached with very stable instruments. We studied the contributors to the centring error in the case of MITHiC and we quantified some of the most important terms.

Keywords: instrumentation: high angular resolution – instrumentation: spectrographs – instrumentation: adaptive optics

Send correspondence to M. El Morsy (mona.elmorsy@lam.fr).

1. INTRODUCTION

In 1995, the first exoplanet was detected and thousands of them have been detected and confirmed since then by indirect or direct methods.[1] The characterisation of these exoplanets remains essential to understanding their atmospheric composition,[2] and their formation and evolution mechanisms.[3] High-contrast imaging (HCI) currently focuses on the direct detection of young ($< 300\,Myr$) giant ($> 1\,M_{\rm Jup}$) exoplanets orbiting at large orbital separation ($> 10\,au$) from their host star. The high contrast (> 10 mag) and small angular separation ($< 1''$) of these planets with respect to their host star are a severe limitation to their detection, but especially to their atmospheric characterisation.

High contrast imaging combines coronagraphy and extreme adaptive optics[4] techniques to respectively attenuate the on-axis stellar light[5,6] and to compensate for the atmospheric distortion in ground-based observations. However, HCI is limited by quasi-static speckles in the focal plane,[7] which emulate the planetary signal. To overcome this constraint, a new generation of exoplanet imagers has been implemented on large ground-based telescopes such as VLT/SPHERE,[8] Gemini/GPI,[9] and Subaru/SCExAO[10] to great success. Nevertheless, the spectral resolution of these instruments (e.g., $R = \lambda/\Delta\lambda = 50$ for IFS/SPHERE) are a limitation to characterise exoplanets.[11]

The characterisation of exoplanets atmosphere using infrared spectrographs such as Keck/NIRSPEC[12] or VLT/CRIRES[13] has been performed using high dispersion spectroscopy (HDS). For ground based observation, HDS in the near-infrared (NIR) had proven to be a powerful technique to retrieve key information of transiting exoplanets[14] and to spectrally resolve molecular features of species in the atmosphere of exoplanets.[15] In 2014, VLT/CRIRES detected the CO lines at 2.3 μm in β Pictoris b using the combination of the MACAO AO system[16] and the implementation of medium-to high-spectral resolution ($R = 100000$ in the H band), which constrained β Pictoris b's rotational velocity and orbital motion.[2] In order to reproduce CRIRES feat, it would be necessary to have access to high-resolution spectrographs supplied with extreme adaptive optics, however, such instruments do not currently exist.

Recently, the combination of high-contrast imaging and high dispersion spectroscopy, named high dispersion coronagraphy (HDC) have started to rise as a robust technique to directly characterise young giant exoplanets.[17] For ground based observations, the combination of HCI and HDS can in theory reach a planet–star contrast of 10^{-7} or better[18] and several on-going projects have implemented HDC on existing telescopes such as Keck/KPIC,[19] Subaru/REACH,[20] and VLT/HiRISE.[21]

The aim of these three projects, amongst others, consists of coupling existing high-contrast instruments with medium to high resolution spectrographs using single mode fibres (SMF).[22] SMFs are advantageous for feeding light into spectrographs due to their precision and stability properties. They are usually used in the focal planes of telescopes due to their spatial filtering c apabilities.[23] However, efficiently coupling a point spread function (PSF) into a SMF is challenging, mainly due to the fact that they only accept a quasi-Gaussian fundamental mode. Furthermore, the central obstruction and spiders on ground-based telescopes significantly affect the coupling efficiency, typically the VLT offers a maximum coupling efficiency of ~73%.[24]

In order to maximise the coupling efficiency of the telescope PSF into a SMF in the context of HiRISE, Otten et al.[24] demonstrate that the PSF must be centred with the core of the fibre within $0.1\,\lambda/D$ to achieve a coupling efficiency better that 95% of the maximally achievable. Any offset impacts the coupling, in the case of the High-Resolution Imaging and Spectroscopy of Exoplanets (HiRISE), we can tolerate a coupling efficiency as low of 59% of the maximum, which corresponds to an offset between the PSF and the SMF of $0.2\,\lambda/D$.

HiRISE offers a very unique opportunity at the VLT to couple two flagship instruments implemented on the Nasmyth platforms of the unit telescope 3 (UT3): the exoplanet imager SPHERE on one side, and the NIR high-resolution spectrograph CRIRES+[25] on the other side. HiRISE aims to link SPHERE and CRIRES+ with optical fibre to achieve the characterisation of known directly imaged young giant exoplanets at a spectral resolutions up to $R = 100000$ in H-band.

HiRISE will take advantage of both SPHERE and CRIRES+ capabilities in H-band to act as a HDC instrument and is composed of three independent parts: (i) the fibre injection module (FIM) that will be implemented downstream of the ExAO and Lyot stop wheel in the IFS arm of SPHERE, (ii) the fibre bundle (FB) that will link SPHERE and CRIRES+, and (iii) the fibre extraction module (FEM) that will be installed on the calibration stage of CRIRES+.

The main challenge of HiRISE is to blindly centre the planet's PSF on top the SMF located in the FB, ideally with an accuracy better than $0.1\,\lambda/D$. The FIM plays a key role during observations since it will pick up the planet's PSF and inject

it into a SMF. Therefore, different strategies are investigated and presented in this paper to fulfil the centring requirement for HiRISE.

In this proceeding three different strategies are investigated to fulfil the required centring specification for HiRISE. To explore these strategies we used an upgraded version of the Marseille Imaging Testbed for High-Contrast (MITHiC).[26] In Sect. 2 we present a brief overview of HiRISE and we describe the PSF centring strategy procedures. In Sect. 3 we present the MITHiC testbed and detail the description of the FIM located on MITHiC. We also explain the characterisation of the setup and the specifications required for the centring strategies. In Sect. 4, we introduce the description of the centring strategy procedures in laboratory, and we discuss the performance results. Finally, in Sect. 5 we conclude.

2. HIGH DISPERSION CORONAGRAPHY IN THE CASE OF HIRISE

2.1 Description of HiRISE

HiRISE redirects the SPHERE/IFS beam and injects the light of a known exoplanet into a SMF connected to the NIR spectropgraph CRIRES+. The FIM is inserted as a vertical bench on the IFS arm of SPHERE, where a pick-off mirror redirect the light towards the FIM instead of the IFS as shown in Fig. 1. Then, the SPHERE pupil is reimaged onto a mirror mounted on a S335 piezo-tip-tilt platform from *Physik Instrumente* and the beam is recollimated thanks to a custom achromatic doublet. The light goes through a dichroic filter that reflects the YJ bands to the tracking camera arm and transmits the H band to the fibres arm. The tracking camera is a C-RED 2 camera from *First Light Imaging*, the image is formed in the focal plane of the tracking camera at F/40 and is Nyquist-sampled at 12.25 mas/pix. In the injection arm, the beam is refocused using an air gap doublet at F/3.5 that matches the numerical aperture (NA = 0.16) of the on-axis science fibre implemented in the fibre bundle. Furthermore, three additional fibres, implemented off-axis are used to sample the stellar light in the speckle field and four 'feedback fibres' are connected to a calibration source and are used to retro inject light into the optical setup. The outputs of the feedback fibres are reimaged on the tracking camera superimposed on the science image, the position of the feedback fibres with respect to the science fibre position acts as a possible approach to accurately centre the planet's PSF onto the science fibre. After the alignment of the system, the FB remains static and the tip-tilt mirror is used to move the focal plane with respect to the science fibre to place the planet's PSF onto the fibre.

2.2 Description of the centring strategies

The role of the FIM consists in centring the planet's PSF on the science fibre with the required accuracy. Due to S/N constraints, the planet's PSF will not be visible on the tracking camera, thus, the planet's acquisition will be performed blindly based on its known relative astrometry with respect to the stellar PSF and the calibrations carried out during the day.

The choice to investigate only three strategies and select the best one to implement for HiRISE have been driven by the fact that the strategies require only a limited amount of hardware and they are usable from the operational point of view at the VLT.

- The first strategy (Fig. 2, top row):
  It relies only on a centring fibre located close to the science fibre. The first step in a non coronagraphic configuration consists on coarsely place the stellar PSF onto the centring fibre. The following step is to refine the position with an optimisation algorithm that maximises the coupling efficiency of the stellar PSF in the centring fibre (Fig. 2, panel 2). Then, by applying the pre-calibrated offset (Fig. 2, panel 1), we place the stellar PSF into the science fibre (Fig. 2, panel 4). Finally, by using the interaction matrix and the astrometry offsets (right ascension and declination), we apply the corresponding offset to the tip-tilt mirror to place the planet on the science fibre (Fig. 2, panel 5).

- The second strategy (Fig. 2, middle row):
  It uses the science fibre and the four feedback fibres in the non coronagraphic configuration. In theory, the diagonal intersection ($\mathcal{I}$) of the four feedback fibres reimaged on the tracking camera provides the position of the science fibre. The first step consists on switching on the four feedback fibres and acquire an image with the tracking camera, find the intersection ($\mathcal{I}$) and determine the position of the science fibre (Fig. 2, panel 2). An offset may occur between $\mathcal{I}$ and the position of the science fibre. It is due to an alignment mismatch between the science arm and the retro-injection arm, and would need to be calibrated beforehand during the laboratory validation of the instrument (Fig. 2, panel 1). Then, by moving the tip-tilt mirror, we place the stellar PSF onto the science fibre and by applying an offset

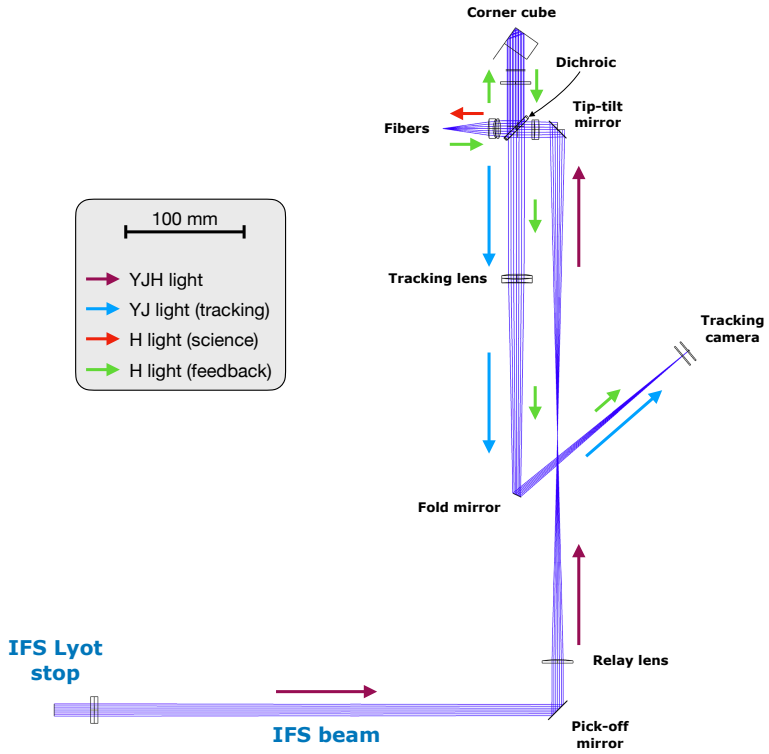

Figure 1: Schematic of the design of the HiRISE/FIM. Reproduced with permission from El Morsy et al.[27]

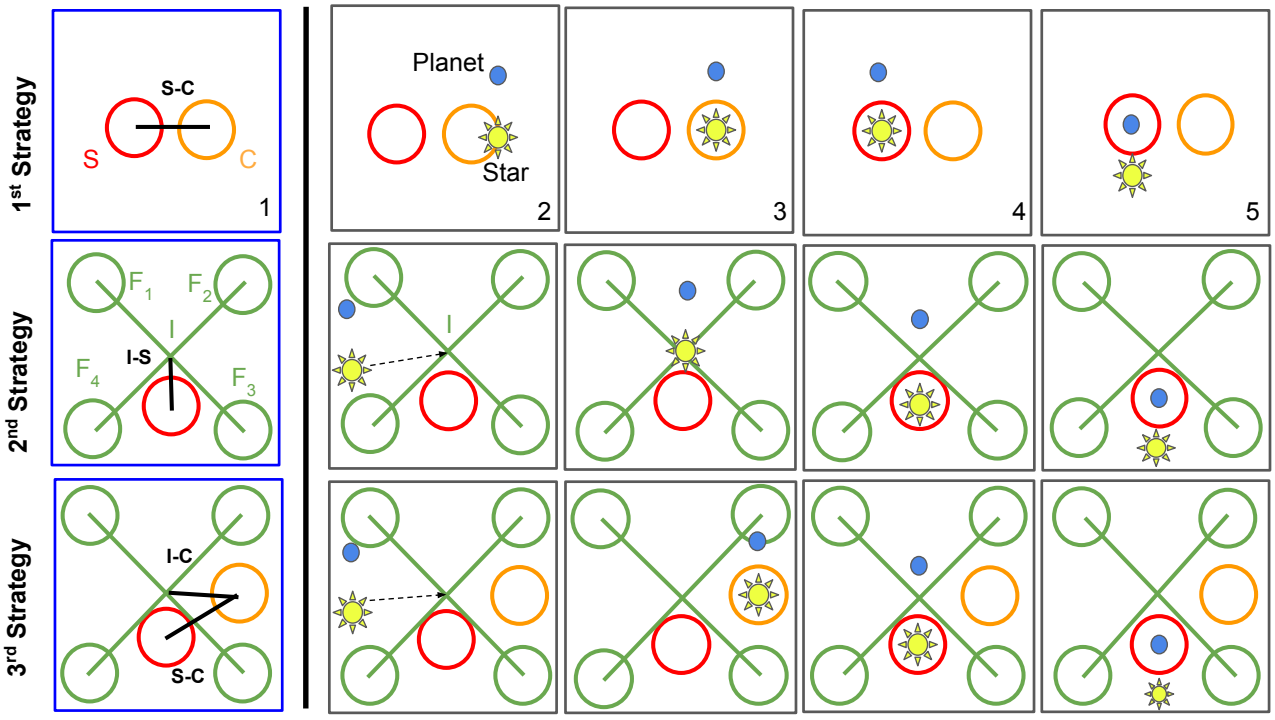

Figure 2: Centring strategy schemes. Each row represents a strategy. The blue frames represent the calibration procedure for each strategy, while the black frames are assigned to the centring procedure. The panels labelled 1–5 show the steps followed to place the planet's PSF into the science fibre. Reproduced with permission from El Morsy et al.[27]

as described for the first strategy (Fig. 2, panel 4), we finally move the planet's PSF into the science fibre (Fig. 2, panel 5).

- The third strategy (Fig. 2, bottom row):
  It combines the first and the second strategy using all the fibres mentioned below. The first step consists in switching on the feedback fibres and to retrieve the intersection ($\mathcal{I}$) (Fig. 2, panel 2). The tip-tilt mirror is use to place the stellar PSF into the centring fibre (Fig. 2, panel 3). Then, we use the pre-calibrated offset (Fig. 2, panel 1) to move the star onto the science fibre science fibre (Fig. 2, panel 4) and finally, we apply an offset to place the planet onto the science fibre (Fig. 2, panel 5).

In HiRISE, the science fibre $\mathcal{S}$ will be connected to CRIRES+ preventing any verification of the planet's injection in the fibre during the o bservation. The challenge to accurately centre the planet's PSF into the science fibre relies on the calibration accuracy performed at each procedure step. In the first strategy, the challenge is to accurately centre the stellar PSF onto the centring fibre, while for the second and the third strategies the crucial first step consists of placing the stellar PSF on the intersection $\mathcal{I}$.

3. FIBER INJECTION INTO A SMF ON THE MITHIC TESTBED

3.1 Description of MITHiC

MITHiC is a HCI testbed located at the Laboratoire d'Astrophysique de Marseille (LAM). It is composed of a telescope simulator (TS), a wavefront sensor (WFS) to measure and compensate for the non-common aberrations (NCPA), a classical Lyot coronagraph (CLC) as shown in Fig. 3. The stellar PSF is generated by the TS through a polarised monochromatic fibre-coupled super-luminescent diode at a wavelength of 670.7 nm. The spatial light modulator (SLM), placed in the pupil plane allows to apply in closed-loop a phase correction to flatten the w avefront. On MITHiC, the creation of an off-axis planet is not feasible, so the SLM is used to create satellite spots. The WFS is a Zernike wavefront sensor called ZELDA.[26]

We modified MITHiC by implementing the FIM in order to emulate the setup that will be implemented on HiRISE. In the foreground of Fig. 4, we can see the implementation of the FIM. A mirror glued on a piezo tip-tilt mount (PI-S335) was used to re-image the pupil of the bench. The mirror is located after the WFS stage and is oriented at 45 °with respect to the optical axis Fig. 4 (blue inset). The testbed is monochromatic, so we use a 50/50 beam-splitter cube to create two separate arms. In the tracking arm, the stellar PSF is imaged on a Coolsnap HQ2 CCD camera from Teledyne positioned at the focal plane with a 4.26 pixel/(λ/D) sampling. In the injection arm, the beam is refocused using a Thorlabs F810SMA-635 collimator to generate a focal plane image at the tip of the FB.

The FB is a custom bundle manufactured by Thorlabs. It is composed of seven 4.5/125 SMF, 2m length, mounted with one SMA connector in the collimator. In Fig. 4 (purple inset), the fibres are labelled $\mathcal{S}$ for the science fibre, $\mathcal{C}$ for the centring fibre, and $\mathcal{F}$1–4 for the feedback fibres, and one space fibre that is not used in the setup. At the centre of the FB, the seven fibres are separated from each others and the ends of the fibres are FC co nnectors. The $\mathcal{S}$ fibre and the $\mathcal{C}$ fibre are connected to two Thorlabs PM101 power meters with S150C cells to record the injected flux. The $\mathcal{F}$1–4 fibres are fed through a home-built system based on four LEDs controlled by a micro-controller Fig. 4 (yellow inset). The light goes to the collimator that acts as an injector in this configuration, then the beam goes through the beam-splitter cube and is reflected to the system thanks to a plane mirror placed closely behind the beam-splitter cube to avoid differential defocus between the tracking arm and the retro-injection arm.

3.2 Characterisation of the testbed

The MiTHIC testbed is enclosed by aluminium protective panels and is subject to daily variations since it is not controlled either in temperature and humidity. Some active devices located on the testbed contribute to heating it, creating turbulences and frequency vibrations. We noticed a vibration at approximately 56 Hz in fast sampled focal plane images and that was traced to acoustic coupling of a DC power supply near the bench. After moving the DC power supply, the 56 Hz signal fell to the background level as shown in Fig. 5. However, even if these disturbances have been attenuated some effects remain and contribute to the limitation of the testbed.

Some impacting terms contribute to the limitation of the testbed and are quantified in this section. The jitter of the PSF, intrinsic to the turbulence or the vibration within the enclosure, is estimated at 0.04 λ/D. The PSF's drift computed from the standard deviation is estimated for both X and Y axis to 0.02 λ/D over 30 min.

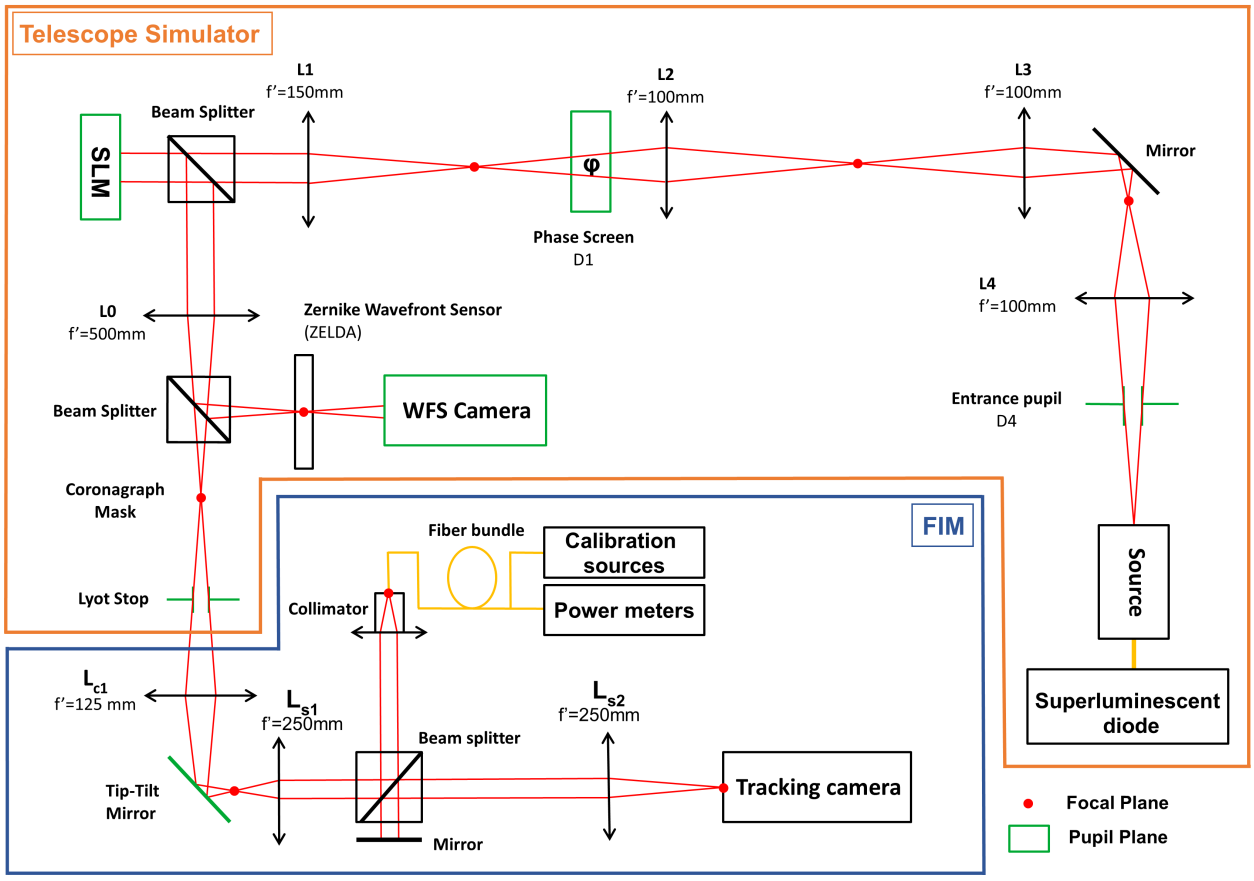

Figure 3: Schematic drawing of the MITHiC testbed. The blue box indicates the fibre injection module (FIM) and the orange box indicates the telescope simulator. Focal planes are represented as red dots and pupil planes are in green. The bench control computer is not represented. The scale and distances between optics are not respected in this drawing. Reproduced with permission from El Morsy et al.[27]

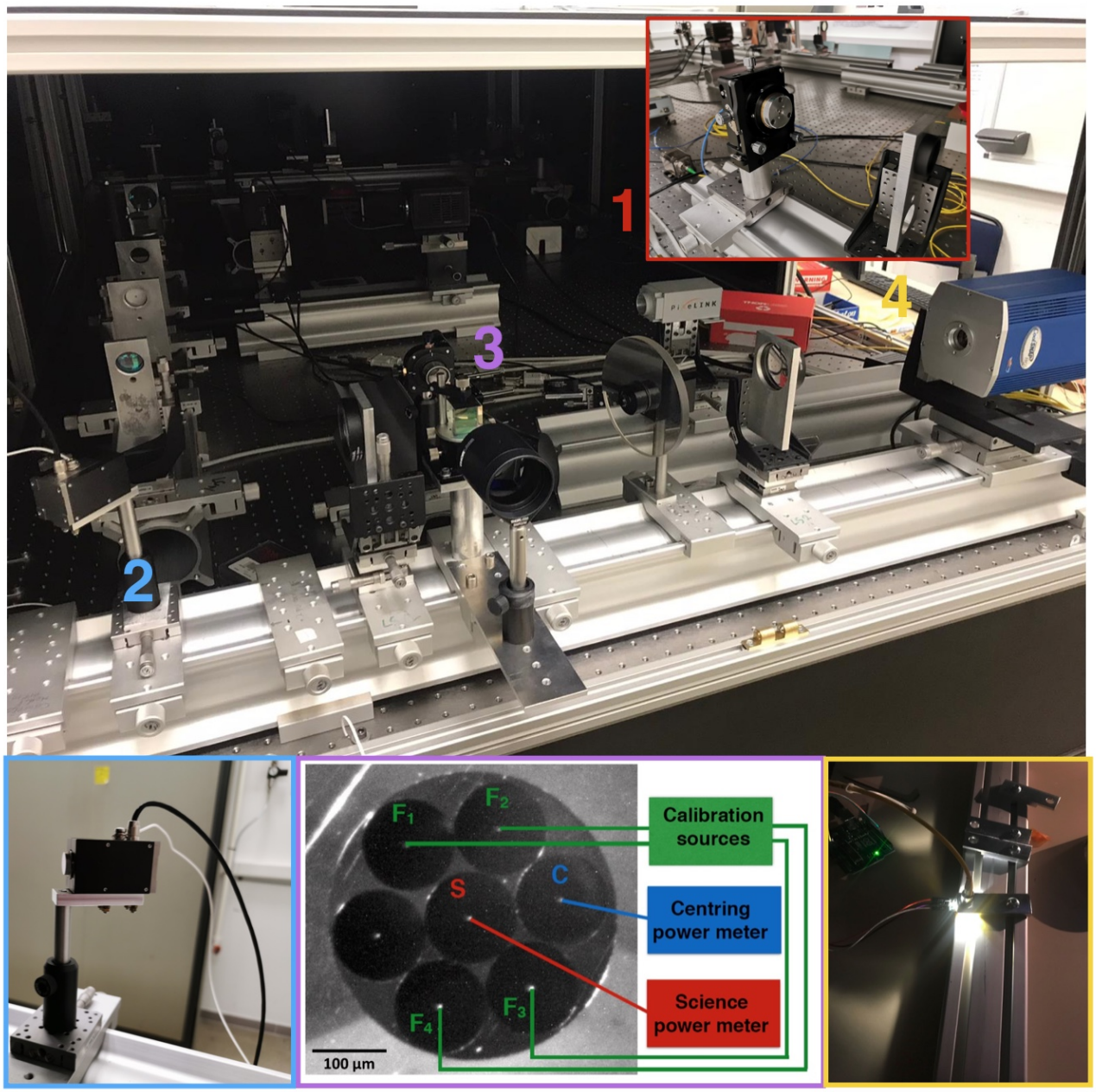

Figure 4: Picture of the MITHiC testbed. The red inset represents the laser source mount used to generate the stellar PSF. In the blue inset, we notice the tip-tilt mirror placed at 45°with regard of the optical axis. The purple inset represents the fibre bundle manufactured by Thorlabs, it is composed of several SMF. Two of these SMFs are connected to two different power meters while four feedback fibres (in green) are connected to calibration sources placed outside of the bench. The yellow inset shows the home-build setup used to retro-inject light into the four feedback fibres.

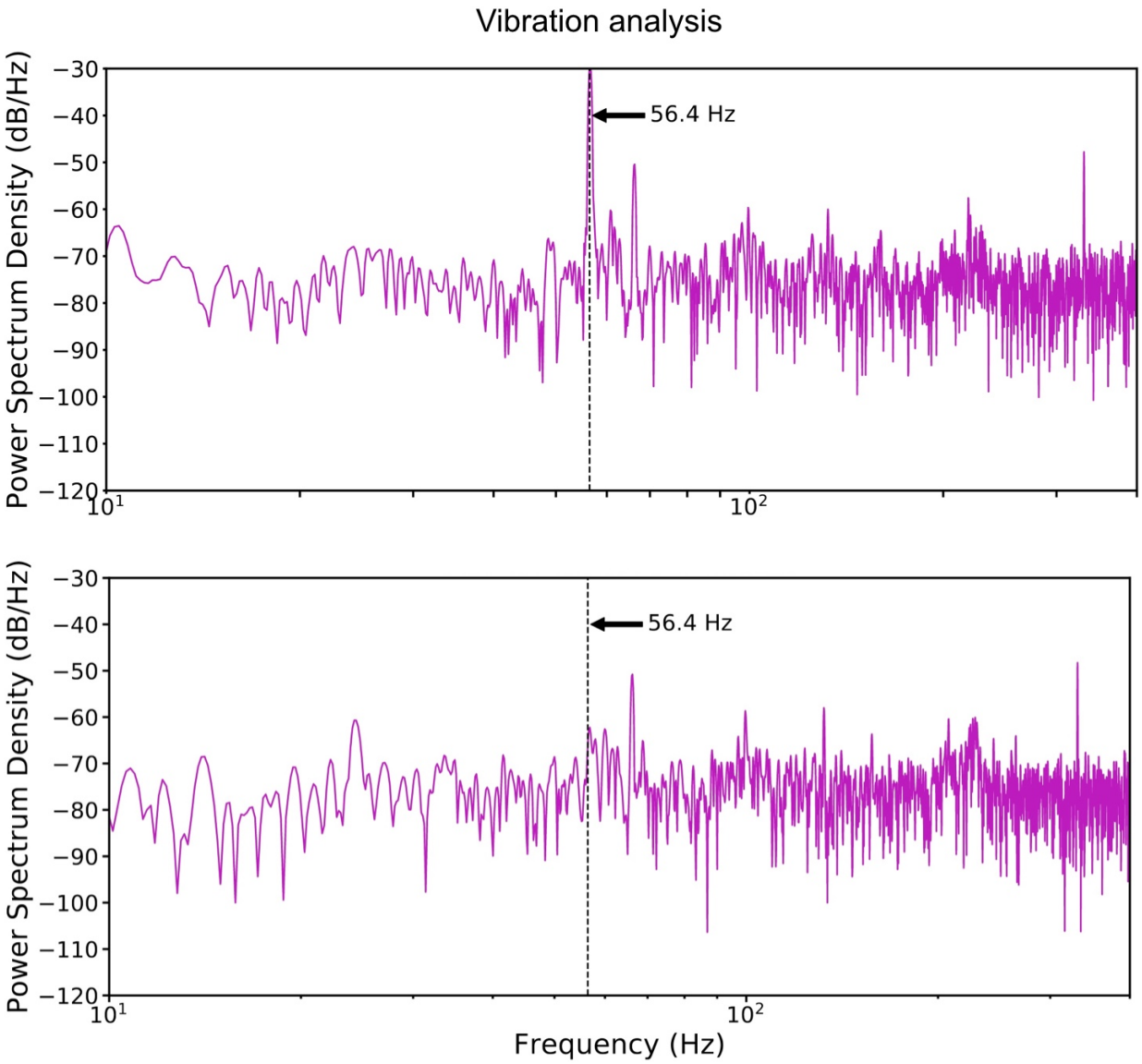

Figure 5: Power spectral density (PSD) plots from experimental data acquired on the MiTHIC testbench. The PSF centroid data is sampled at a high frequency using a tracking camera placed at the focal plane between the L4 lens and the mirror (Fig. 3) and only the PSDs in the X-axis are shown in this figure. The upper panel shows a peak at 56.4 Hz due to the vibration of a nearby electronic device. The lower panel shows the PSD after mitigating steps were undertaken. No major sources of vibration at specific frequencies remain.

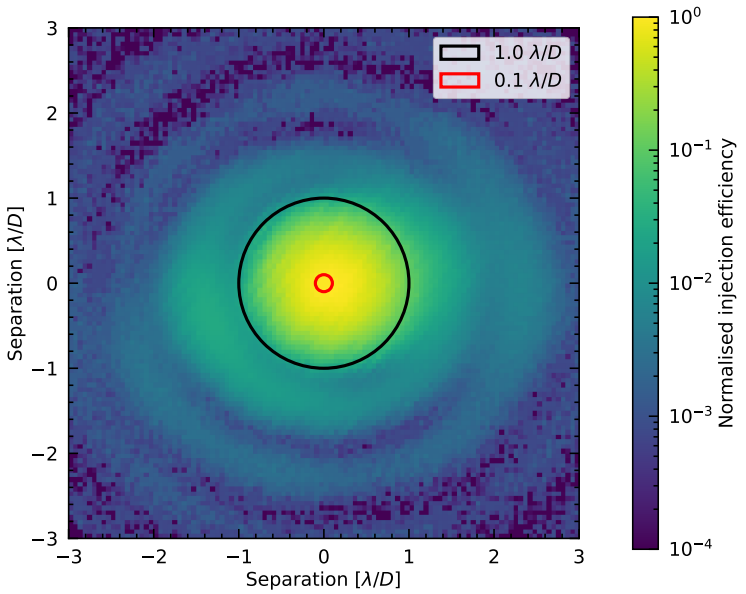

Figure 6: Injection map obtained with the centring power meter by scanning a grid of 6×6 λ/D with a pitch of 0.05 λ/D in both directions. The red circle represents the required accuracy of $0.1\lambda/D$. Reproduced with permission from El Morsy et al.[27]

The static aberration measured by the ZELDA wavefront sensing are estimated at 7 nm RMS in 15 days if the testbed remains in the configuration where the panels are closed. This error term remains not significant for the tests performed on MiTHIC due to the tests timescale.

3.3 Centring specification

The performance of HiRISE is driven by the overall transmission of the system. Injecting light into SMF is inherently challenging and can lead to important flux losses if the centring is not accurate. In Fig. 7 (panel a), we notice that the simulations by Otten et al.[24] show that a centring accuracy of 0.1 λ/D is required for HiRISE. In this case, we expect a maximum peak coupling efficiency loss of five percentage points compared to a perfect centring of the PSF on the science fibre. To illustrate the challenging requirement, we performed an injection map of the stellar PSF into the $\mathcal{C}$ fibre on MITHiC and it is illustrated in Fig. 6. It represents the flux injected into the $\mathcal{C}$ fibre, as measured by the power meter and the two circles delimit the 0.1 λ/D and 1 λ/D around the centre of the fibre. In comparison to the simulations, we computed a radial profile of the injection map, which is shown in Fig. 7 (panel b). It demonstrates that at 0.1 λ/D the loss is estimated to 2.6 percentage points. For HiRISE, an accuracy of 0.2 λ/D could be acceptable but at a cost of a loss of ten percentage points compared to the perfect case.

4. IMPLEMENTATION OF THE CENTRING STRATEGIES ON MITHIC

4.1 Calibrations

- Centre of the fibres:
  In order to retrieve the $\mathcal{S}$ and the $\mathcal{C}$ fibres in the tip-tilt commands space, the first step consists of computing a coarse injection map. To achieve a more accurate determination of the fibres centre, we used the tip-tilt mirror position associated with the maximum of the coarse injection map as an input to a gradient descent algorithm based on a Nelder-Meade approach that maximises the flux injection into the fibres. In this proceeding, the optimisation of the injection based on a gradient algorithm is referred to as an injection optimisation.

- $\mathcal{C}$–$\mathcal{S}$ fibre distance:
  Another important step is to be able to accurately switch between the $\mathcal{C}$ and the $\mathcal{S}$. To fulfil this requirement, an accurate calibration of the $\mathcal{C}$–$\mathcal{S}$ distance is necessary and the results[27] demonstrates that for 100 measurements

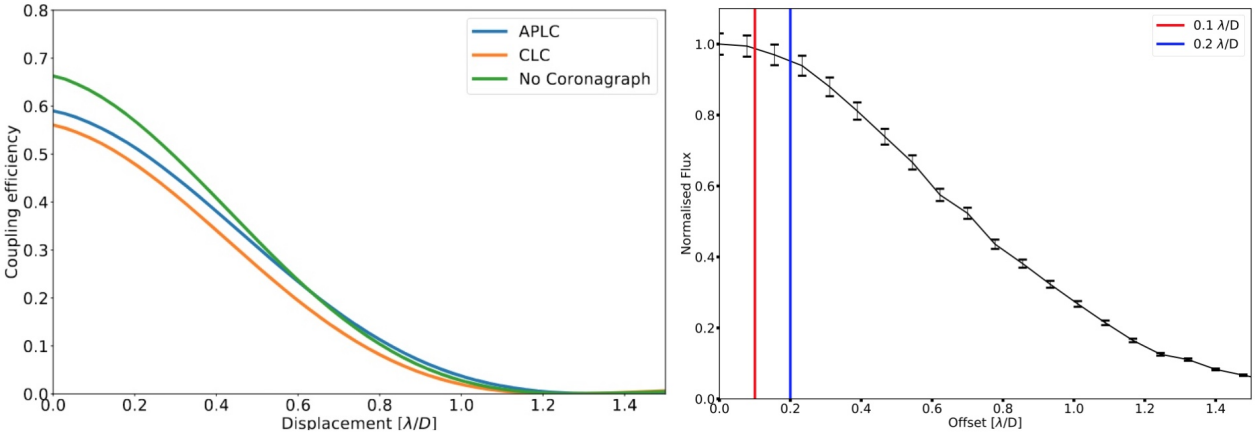

Figure 7: (a) left panel: coupling efficiency as a function of displacement between the PSF core and the Gaussian mode of the fibre simulated for three different coronagraph options and evaluated at 1.6 μm.[24] (b) right panel: radial profile of the injection map computed with the centring fibre on MiTHIC. Reproduced with permission from El Morsy et al.[27]

to calibrate the offset between the two fibres, 99% of the points are within the requirement of 0.1 λ/D. We also noticed that the standard deviation estimation in tip-tilt is 0.02 λ/D, which is approximately equal to the PSF's jitter uncertainty.

- Offset between the retro-injection and tracking arm:
  The calibration fibres $\mathcal{F}$1–4 are retro-fed simultaneously with a LED signal and re-imaged on the tracking camera superimposed on the science image. In theory, the diagonal intersection ($\mathcal{I}$) of the four spots retrieved by a 2D Gaussian fit, should determine the position of the science fibre on the tracking camera. However, the mirror placed behind the beam splitter cube is tilted with respect to the optical axis and introduces an offset between the two arms. For the second strategy, the $\mathcal{I}$–$\mathcal{S}$ offset is accurately measured during the calibration procedure. For the third strategy, the calibration follows the same path, but measures the $\mathcal{I}$–$\mathcal{C}$ offset.

- Accurate positioning of the PSF:
  A calibration is necessary to accurately position the stellar PSF at any coordinate on the tracking camera. To fulfil this necessary calibration, a non linear approach with an interpolation function based on a full 2D calibration of the tip-tilt mirror as seen by the tracking camera is performed. The resulting interpolation function allow to obtain the tip-tilt command to place the stellar PSF at any position in the camera's field of view (FoV). El Morsy et al.[27] computed the residual of the interpolation function as measured on the tracking camera and demonstrated that the residual are quasi-Gaussian with a standard deviation of 0.03 λ/D, which is below 0.1 λ/D and noticed that 97.61% of the residuals fall within $\pm$0.1 λ/D. The stability of the calibration grid used to build the interpolation function relies on the bench stability. It takes approximately 6 minutes to be computed and is stable over approximately 30 minutes due to the PSF's drift estimated at 0.02 λ/D.

- ZELDA calibration:
  The calibration is computed at the beginning of each test as a sanity step and to obtain the best possible PSF quality. A wavefront quality better than 20 nm RMS is typically obtained in normal conditions.

4.2 Data acquisition

We do not have the possibility to create an off-axis point source on MITHiC to simulate a planet so to overcome this constraint, we introduce a sinusoidal modulation on the SLM to create two symmetric satellite spots and take one of these satellite spot as the planet's PSF. The spatial frequency and orientation of the sine wave allow choosing the angular separation and position angle of the planet. The performance tests required several steps to be computed such as (i) measuring the relative star-planet astrometry on the tracking camera image, (ii) evaluating the star-planet contrast ratio. The contrast of a factor 3.48 is modest but does not impact the performance results on-sky because the system is blind to

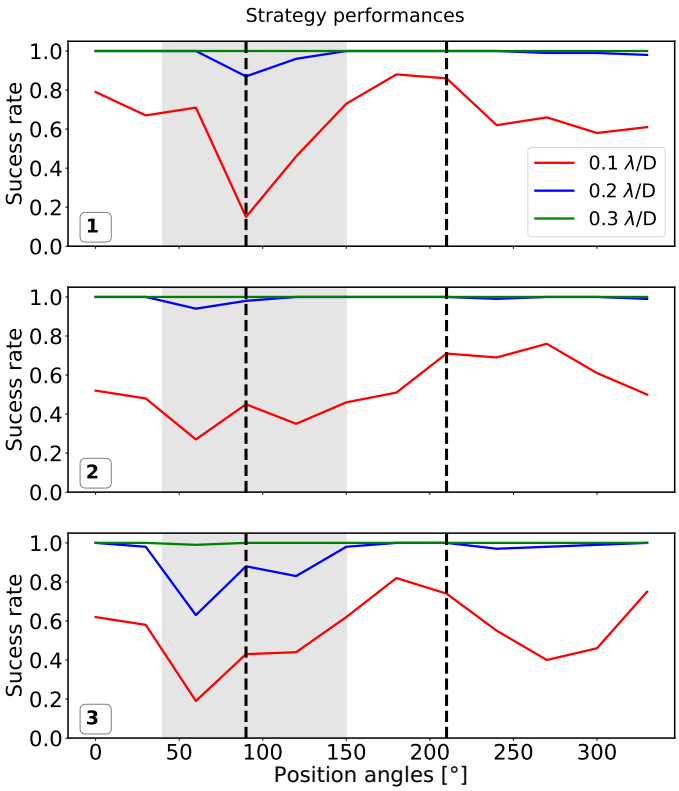

Figure 8: Success rate as a function of position angle around the star. The results for the first, second, and third strategies are plotted in the upper, middle, and lower panels, respectively. The grey area represents the region where a trend is noticed. The black dashed lines at 90° and 210° represent the angles for which additional tests are performed and demonstrated. Reproduced with permission from El Morsy et al.[27]

the planet's signal during the centring procedure. However, the modest contrast in the laboratory is essential to check the final accuracy.

Regardless of the strategy, at the end of each centring procedure a verification optimisation (VO) is performed to gauge how close the planet's PSF is to the centre of the $\mathcal{S}$ fibre. The tip-tilt displacement before and after the optimisation, ϵ, gives a measurement of the distance to the centre. The success or failure status of the performance are defined by the ϵ error and are compared to the specification accuracy of 0.1 λ/D.

4.3 Results

The results for a planet located at different position angles around the star and with an angular separation of 10 λ/D are demonstrated in Fig. 8. The figure shows the success rate of each strategy for three specification accuracies of 0.1, 0.2, and 0.3 λ/D.

For the first strategy we reach an average success rate of 0.7 for the specification accuracy of 0.1 λ/D, and 0.95 or higher for accuracies greater than 0.2 λ/D. For the second strategy the success rate is on average equal to 0.6 for an accuracy of 0.1 λ/D, and again the success rates are higher than 0.95 for an accuracy of 0.2 λ/D and 0.3 λ/D. Finally, the third strategy demonstrates a success rate slightly worse than the first and second strategies.

The second performance tests were performed with planets located at different angular separations; we only tested three position angles: 90° (located in the grey area), 210°, and 330°. The first strategy shows the lowest performance for 90°, with a success rate that decrease as a function of the angular separations. It reaches 0.0 at worst for an accuracy of 0.1 λ/D and 0.2 λ/D, and is lower than 0.4 for an accuracy of 0.3 λ/D. This position angle is identified as problematic in the calibrations and explained in more details in Section 4 of El Morsy et al.[27] For the two other position angles we reach a success rate higher than 0.4 for 0.1 λ/D and higher than 0.95 for an accuracy of 0.2 λ/D and 0.3 λ/D. The trends for

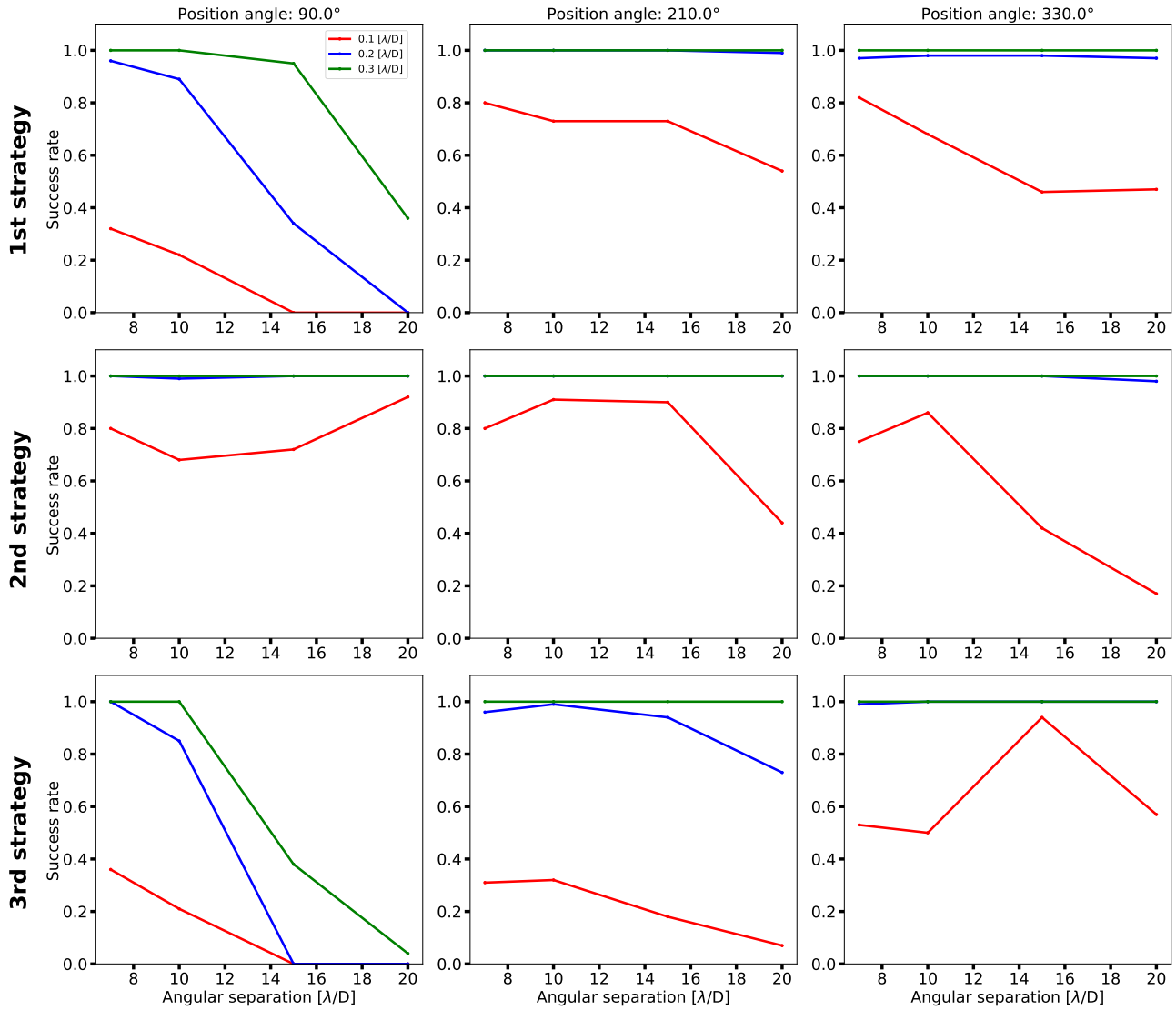

Figure 9: Success rate as a function of the angular separation from the star. The results for the first, second, and third strategies are plotted in the upper, middle, and lower panels, respectively. Reproduced with permission from El Morsy et al.[27]

the first strategy are found also in the results for the third strategy, but with even lower results. Finally, the results for the second strategy are highly better, with significant high rates at all position angles for the 0.2 and 0.3 λ/D specifications, and decreased success rates for a specification of 0.1 λ/D, but not poorly as for the two other strategies.

5. CONCLUSIONS

HiRISE aims to implement a coupling between SPHERE and CRIRES+ at the VLT/UT3. One of the main constraints of HiRISE is to blindly inject a known planet's PSF on the science fibre to transmit it to the spectrograph with the highest possible throughput. Previous studies for HiRISE have determined that a specification of 0.1 λ/D would be the best choice to maximise the transmission.[24]

In order to study the best centring strategy, we used the MITHiC testbed at LAM, which has been upgraded to emulate the setup used in HiRISE. On MITHiC, three strategies were implemented and tested to assess the feasibility of reaching a specification of 0.1 λ/D. We conducted a performance study to verify the planet's PSF centring on the science fibre $\mathcal{S}$

for several angular separations and for several position angles around the star. Regardless of the strategy, we conclude that reaching an accuracy of $0.1\,\lambda/D$ is extremely challenging mainly because it requires a high level of accuracy at every calibration step, which is difficult to reach in a non-optimised system.

Some performance results can be explained by limitations in the system, such as the PSF jitter and the accuracy of the interpolation function. The interpolation function is used in all three strategies to place the stellar PSF at any position in the FoV. Even though 97.61% of the interpolation function's residuals are within the accuracy specification of $\pm 0.1\,\lambda/D$, the presence of outliers negatively impacts the interpolation function in certain areas. These outliers originate from hardware limitations inherent to the MITHiC testbed, which should not be present for HiRISE integrated into SPHERE.

The AIT phase of HiRISE in Europe has started. The alignment of the system is based on a simplified SPHERE simulator that reproduces the main characteristics of the SPHERE IFS beam using off-the-shelf components. This simulator will be used to align the bench and verify the image and wavefront quality. The conclusions regarding the best centring strategy for HiRISE will come from the AIT phase, but the final decision will have to wait the first on-sky tests.

ACKNOWLEDGMENTS

This project has received funding from the European Research Council (ERC) under the European Union's Horizon 2020 research and innovation programme, grant agreements No. 757561 (HiRISE) and from Région Provence-Alpes-Côte d'Azur under grant agreement 2014-0276 (ASOREX project).

REFERENCES

[1] Mayor, M. and Queloz, D., "A jupiter-mass companion to a solar-type star," *Nature* **378**(6555), 355–359 (1995).

[2] Snellen, I. A., Brandl, B. R., De Kok, R. J., Brogi, M., Birkby, J., and Schwarz, H., "Fast spin of the young extrasolar planet β pictoris b," *Nature* **509**(7498), 63–65 (2014).

[3] Crepp, J. R., Johnson, J. A., Fischer, D. A., HOwARD, A. W., Marcy, G. W., Wright, J. T., Isaacson, H., Boyajian, T., Von Braun, K., Hillenbrand, L. A., et al., "The dynamical mass and three-dimensional orbit of hr7672b: a benchmark brown dwarf with high eccentricity," *The Astrophysical Journal* **751**(2), 97 (2012).

[4] Fusco, T., Rousset, G., Sauvage, J.-F., Petit, C., Beuzit, J.-L., Dohlen, K., Mouillet, D., Charton, J., Nicolle, M., Kasper, M., et al., "High-order adaptive optics requirements for direct detection of extrasolar planets: Application to the sphere instrument," *Optics Express* **14**(17), 7515–7534 (2006).

[5] Guyon, O., Pluzhnik, E., Kuchner, M. J., Collins, B., and Ridgway, S., "Theoretical limits on extrasolar terrestrial planet detection with coronagraphs," *The Astrophysical Journal Supplement Series* **167**(1), 81 (2006).

[6] Mawet, D., Pueyo, L., Lawson, P., Mugnier, L., Traub, W., Boccaletti, A., Trauger, J. T., Gladysz, S., Serabyn, E., Milli, J., Belikov, R., Kasper, M., Baudoz, P., Macintosh, B., Marois, C., Oppenheimer, B., Barrett, H., Beuzit, J.-L., Devaney, N., Girard, J., Guyon, O., Krist, J., Mennesson, B., Mouillet, D., Murakami, N., Poyneer, L., Savransky, D., Vérinaud, C., and Wallace, J. K., "Review of small-angle coronagraphic techniques in the wake of ground-based second-generation adaptive optics systems," in [*Space Telescopes and Instrumentation 2012: Optical, Infrared, and Millimeter Wave*], Clampin, M. C., Fazio, G. G., MacEwen, H. A., and Jr., J. M. O., eds., **8442**, 62 – 82, International Society for Optics and Photonics, SPIE (2012).

[7] Soummer, R., Ferrari, A., Aime, C., and Jolissaint, L., "Speckle noise and dynamic range in coronagraphic images," *The Astrophysical Journal* **669**(1), 642 (2007).

[8] Beuzit, J.-L., Vigan, A., Mouillet, D., Dohlen, K., Gratton, R., Boccaletti, A., Sauvage, J.-F., Schmid, H. M., Langlois, M., Petit, C., et al., "Sphere: the exoplanet imager for the very large telescope," *Astronomy & Astrophysics* **631**, A155 (2019).

[9] Macintosh, B., Graham, J. R., Ingraham, P., Konopacky, Q., Marois, C., Perrin, M., Poyneer, L., Bauman, B., Barman, T., Burrows, A. S., et al., "First light of the gemini planet imager," *proceedings of the National Academy of Sciences* **111**(35), 12661–12666 (2014).

[10] Jovanovic, N., Martinache, F., Guyon, O., Clergeon, C., Singh, G., Kudo, T., Garrel, V., Newman, K., Doughty, D., Lozi, J., et al., "The subaru coronagraphic extreme adaptive optics system: enabling high-contrast imaging on solar-system scales," *Publications of the Astronomical Society of the Pacific* **127**(955), 890 (2015).

[11] Zurlo, A., Vigan, A., Mesa, D., Gratton, R., Moutou, C., Langlois, M., Claudi, R. U., Pueyo, L., Boccaletti, A., Baruffolo, A., and et al., "Performance of the vlt planet finder sphere," *Astronomy & Astrophysics* **572**, A85 (Dec 2014).

[12] McLean, I. S., Becklin, E. E., Bendiksen, O., Brims, G., Canfield, J., Figer, D. F., Graham, J. R., Hare, J., Lacayanga, F., Larkin, J. E., et al., "Design and development of nirspec: a near-infrared echelle spectrograph for the keck ii telescope," in [*Infrared Astronomical Instrumentation*], **3354**, 566–578, International Society for Optics and Photonics (1998).

[13] Kaeufl, H.-U., Ballester, P., Biereichel, P., Delabre, B., Donaldson, R., Dorn, R., Fedrigo, E., Finger, G., Fischer, G., Franza, F., Gojak, D., Huster, G., Jung, Y., Lizon, J.-L., Mehrgan, L., Meyer, M., Moorwood, A., Pirard, J.-F., Paufique, J., Pozna, E., Siebenmorgen, R., Silber, A., Stegmeier, J., and Wegerer, S., "CRIRES: a high-resolution infrared spectrograph for ESO's VLT," in [*Ground-based Instrumentation for Astronomy*], Moorwood, A. F. M. and Iye, M., eds., *Society of Photo-Optical Instrumentation Engineers (SPIE) Conference Series* **5492**, 1218–1227 (Sept. 2004).

[14] Snellen, I. A., De Kok, R. J., De Mooij, E. J., and Albrecht, S., "The orbital motion, absolute mass and high-altitude winds of exoplanet hd 209458b," *Nature* **465**(7301), 1049–1051 (2010).

[15] Brogi, M., Snellen, I., De Kok, R., Albrecht, S., Birkby, J., and De Mooij, E., "Detection of molecular absorption in the dayside of exoplanet 51 pegasi b?," *The Astrophysical Journal* **767**(1), 27 (2013).

[16] Arsenault, R., Alonso, J., Bonnet, H., Brynnel, J., Delabre, B., Donaldson, R., Dupuy, C., Fedrigo, E., Farinato, J., Hubin, N. N., Ivanescu, L., Kasper, M. E., Paufique, J., Rossi, S., Tordo, S., Stroebele, S., Lizon, J.-L., Gigan, P., Delplancke, F., Silber, A., Quattri, M., and Reiss, R., "MACAO-VLTI: An Adaptive Optics system for the ESO VLT interferometer," in [*Adaptive Optical System Technologies II*], Wizinowich, P. L. and Bonaccini, D., eds., *Society of Photo-Optical Instrumentation Engineers (SPIE) Conference Series* **4839**, 174–185 (Feb. 2003).

[17] Riaud, P. and Schneider, J., "Improving earth-like planets' detection with an elt: the differential radial velocity experiment," *Astronomy & Astrophysics* **469**(1), 355–361 (2007).

[18] Snellen, I., de Kok, R., Birkby, J. L., Brandl, B., Brogi, M., Keller, C., Kenworthy, M., Schwarz, H., and Stuik, R., "Combining high-dispersion spectroscopy with high contrast imaging: Probing rocky planets around our nearest neighbors," *Astronomy & Astrophysics* **576**, A59 (Apr. 2015).

[19] Delorme, J.-R., Jovanovic, N., Echeverri, D., Mawet, D., Kent Wallace, J., Bartos, R. D., Cetre, S., Wizinowich, P., Ragland, S., Lilley, S., Wetherell, E., Doppmann, G., Wang, J. J., Morris, E. C., Ruffio, J.-B., Martin, E. C., Fitzgerald, M. P., Ruane, G., Schofield, T., Suominen, N., Calvin, B., Wang, E., Magnone, K., Johnson, C., Sohn, J. M., López, R. A., Bond, C. Z., Pezzato, J., Sayson, J. L., Chun, M., and Skemer, A. J., "Keck Planet Imager and Characterizer: a dedicated single-mode fiber injection unit for high-resolution exoplanet spectroscopy," *Journal of Astronomical Telescopes, Instruments, and Systems* **7**, 035006 (July 2021).

[20] Kotani, T., Kawahara, H., Ishizuka, M., Jovanovic, N., Guyon, O., Vievard, S., Lozi, J., Sahoo, A., Yoneta, K., and Tamura, M., "The reach project: combining extremely high-contrast and high spectral resolution at the subaru telescope," in [*Adaptive Optics Systems VII*], **11448**, 1144878, International Society for Optics and Photonics (2020).

[21] Vigan, A., Otten, G., Muslimov, E., Dohlen, K., Philipps, M., Seemann, U., Beuzit, J.-L., Dorn, R., Kasper, M., Mouillet, D., et al., "Bringing high-spectral resolution to vlt/sphere with a fiber coupling to vlt/crires+," in [*Ground-based and Airborne Instrumentation for Astronomy VII*], **10702**, 1070236, International Society for Optics and Photonics (2018).

[22] Jovanovic, N., Schwab, C., Guyon, O., Lozi, J., Cvetojevic, N., Martinache, F., Leon-Saval, S., Norris, B., Gross, S., Doughty, D., et al., "Efficient injection from large telescopes into single-mode fibres: Enabling the era of ultra-precision astronomy," *Astronomy & Astrophysics* **604**, A122 (2017).

[23] Ghasempour, A., Kelly, J., Muterspaugh, M. W., and Williamson, M. H., "A single-mode echelle spectrograph: eliminating modal variation, enabling higher precision doppler study," in [*Modern Technologies in Space-and Ground-based Telescopes and Instrumentation II*], **8450**, 845045, International Society for Optics and Photonics (2012).

[24] Otten, G., Vigan, A., Muslimov, E., N'Diaye, M., Choquet, E., Seemann, U., Dohlen, K., Houllé, M., Cristofari, P., Phillips, M., et al., "Direct characterization of young giant exoplanets at high spectral resolution by coupling sphere and crires+," *Astronomy & Astrophysics* **646**, A150 (2021).

[25] Dorn, R. J., Follert, R., Bristow, P., Cumani, C., Eschbaumer, S., Grunhut, J., Haimerl, A., Hatzes, A., Heiter, U., Hinterschuster, R., et al., "The"+" for crires: enabling better science at infrared wavelength and high spectral resolution at the eso vlt," in [*Ground-based and Airborne Instrumentation for Astronomy VI*], **9908**, 99080I, International Society for Optics and Photonics (2016).

[26] Pourcelot, R., Vigan, A., Dohlen, K., Rouzé, B., Sauvage, J.-F., El Morsy, M., Lopez, M., N'Diaye, M., Caillat, A., Choquet, E., et al., "Calibration of residual aberrations in exoplanet imagers with large numbers of degrees of freedom," *Astronomy & Astrophysics* **649**, A170 (2021).

[27] Morsy, M. E., Vigan, A., Lopez, M., Otten, G. P. P. L., Choquet, E., Madec, F., Costille, A., Sauvage, J. F., Dohlen, K., Muslimov, E., Pourcelot, R., Floriot, J., Benedetti, J. A., Blanchard, P., Balard, P., and Murray, G., "Validation of strategies for coupling exoplanet psfs into single-mode fibres for high-dispersion coronagraphy," *Astronomy & Astrophysics* (in press).